International Journal of Thermal Sciences 49 (2010) 702–713

Contents lists available at ScienceDirect

International Journal of Thermal Sciences

journal homepage: www.elsevier.com/locate/ijts

Endwall heat transfer and pressure drop in scale-roughened pin-fin channels

Shyy Woei Chang [a,*,1], Arthur William Lees [b,2]

[a] Thermal Fluids Laboratory, National Kaohsiung Marine University, No. 142, Haijhuan Road, Nanzih District, Kaohsiung City 81143, Taiwan, ROC
[b] School of Engineering, Swansea University, Singleton Park, Swansea, South Wales, SA2 8PP, UK

ARTICLE INFO

Article history:
Received 16 December 2008
Received in revised form
9 June 2009
Accepted 25 September 2009
Available online 12 October 2009

Keywords:
Compound scaled roughness
and pin-fin array
Heat transfer augmentation

ABSTRACT

There is a growing requirement for improved heat transfer performance for a number of electronic devices and this dictates a need to further elevate the endwall heat transfer performances for pin-fin channels. Driven by this need, a novel compound heat transfer enhancement (HTE) measure that combines deepened scales and pin-fin array is devised. Characteristics of heat transfer and pressure drop performances in two scale-roughened pin-fin channels with two different pin pitch-to-diameter ratios are compared for both forward and backward flows in the Reynolds Number (*Re*) range of 1000–30000. Comparisons of heat transfer data, pressure drop measurements and thermal performance factors with previous results collected from a variety of single and compound HTE devices demonstrate the significant augmentations in both heat transfer rates and pressure drop coefficients for the present HTE measure. This present compound HTE measure with scales and pin-fin array demonstrates an enhancement on the heat transfer up to of 22 times of the developed flow references in smooth-walled pipe within the *Re* range of 1000–30000. Experimental correlations of heat transfer and pressure-drop coefficients for two scale-roughened pin-fin channels with forward and backward flows are derived to assist design applications.

1. Introduction

As a passive heat transfer enhancement (HTE) measure, pin-fins enhance structure integrity, increase heat transfer areas via fin effects and induce horseshoe vortices at the pin-endwall junctions hence facilitating HTE impacts. These features are widely fitted in the cooling passages at the trailing edge of a gas turbine blade and in the heat sink for cooling of electronic chipsets to enhance the heat transfer. Driven by these cooling applications, a large number of experimental and numerical studies examined heat transfer performances over the pin-fins and endwalls in the pin-fin channels [1–16]. These pin-fins improve heat transfer performances by tripping wakes which enhance fluid mixing but with consequential increase in pressure gradients and friction drag. The pin-to-endwall junctions and each pin-row give rise to a number of complex vortex structures that augment endwall heat transfer rates. In this respect, the horseshoe vortices initiated upstream each pin at the pin-endwall junctions are of the primary importance for regional endwall HTE effects [1]. At locations upstream the leading edges of pin-fins on the endwall, two legs of each horseshoe vortex separate and roll around the adjoining pin that advect downstream to form the pin-fin wakes [2]. These wakes re-circulate the fluids behind each pin and generate low heat transfer regions there. Adverse pressure gradients are simultaneously developed as flows traverse each pin that considerably elevates the pressure drop penalties. The separated shear layers induced by these vortical flows reattach after the recirculation zone and re-elevate local heat transfer rates near the reattachment points. Along with the downstream growth of the HTE mechanisms tripped by pin-fins, the boundary layers develop over each endwall. The endwall heat transfer performances along a pin-fin channel are indicative of the trade-offs between the streamwise enhanced HTE mechanisms tripped by pin-fins against the thickened endwall boundary layers. As a result of such trade-offs, the endwall Nusselt number (*Nu*) increases progressively in the downstream direction over the first 3–4 pin-rows prior to the so-called periodically developed flow region. The different flow conditions generated over the endwall and around the outer surface of each pin-fin generally provide the higher HTE effects on the pin surfaces by 35% [3] or 10–20% [4] over those on the endwall.

While the aforementioned flow physics generalizes the heat transfer characteristics in a pin-fin channel, the detailed HTE effects vary with the height-to-diameter ratio [5,6] and the shape [7–11] of pins, the arrangement [12,13] and the orientation [14] of pin-arrays

* Corresponding author. Tel.: +886 7 8100888 5216; fax: +86 886 7 571 60 13.
E-mail address: swchang@mail.nkmu.edu.tw (S.W. Chang).
[1] Visiting Professor to Swansea University, 2008–2009.
[2] Tel.: +44 1792 205678.

1290-0729/$ – see front matter © 2009 Elsevier Masson SAS. All rights reserved.
doi:10.1016/j.ijthermalsci.2009.09.008

Nomenclature

English Symbols

A,n,E,F,G	Correlation coefficients
Cp	Constant specific heat ($Jkg^{-1}K^{-1}$)
D	Diameter of scale (m)
D_P	Pin diameter (m)
D_S	Diameter of scale (m)
d	Hydraulic diameter of the test channel (m)
e_S	Depth of scale (m)
f	Pressure drop (Fanning friction) factor $= [\Delta P/(0.5\rho W_m^2)]/(d/4L)$
f_∞	Fanning friction factor for developed flow in smooth walled plain tube
H	Channel height (m)
H_P	Pin height (m)
k_f	Thermal conductivity of fluid ($Wm^{-1}K^{-1}$)
L	Channel length (m)
Nu	Local Nusselt number $= qd/k_f(T_w - T_b)$
$\overline{Nu}$	Averaged Nusselt number for developed flow
Nu_∞	Nusselt number value for developed flow in smooth walled plain tube
P_P	x-wise pin-pitch (m)
P_S	Skew-wise pin-pitch (m)
P_r	Prandtl number $= \mu Cp/k_f$
ΔP	Pressure drop across entire test channel (Nm^{-2})
q	Convective heat flux (Wm^{-2})
Re	Reynolds number $= \rho W_m d/\mu$
S	y-wise pin-pitch (m)
S_P	Scale pitch (m)
T_b	Fluid bulk temperature (K)
T_w	Wall temperature (K)
W	Channel width (m)
W_m	Mean flow velocity (ms^{-1})
x, y	Coordinate system referred to midway of flow entry as origin (m)

Greek Symbols

α_S	Scale attack angle (degrees)
ρ	Density of fluid (kgm^{-3})
μ	Fluid dynamic viscosity ($kgm^{-1}s^{-1}$)
η	Thermal performance factor $= (\overline{Nu}/Nu_\infty)/(f/f_\infty)^{1/3}$

and the clearance between endwall and detached pins [15,16]. In view of the endwall heat transfer performance, the staggered diamond pin-fin array with pitch ratios of 1.5–2.5 pin-diameters offers considerable HTE effects; while the elliptical fins provide higher thermal performance factors [13]. Among the various pin-fin geometries, the circular pin-fins are most extensively adopted for cooling of gas turbine blades that offer the endwall Nu elevations in the general ranges between 2 and 3.2 times of the Dittus-Boelter Nusselt number levels (Nu_∞) [2]. The adverse pressure gradients around each pin and the increased friction drag over a pin-fin array have increased the pressure-drop penalties substantially. Therefore previous work utilized the detached pin-fins [16] as an attempt to reduce the pressure drop coefficients in the pin-fin channels by eliminating the adverse pressure gradients at the pin-endwall junctions. The accelerated flow through the small clearance between the endwall and each detached pin replaces the diminished horseshoe vortices as an alternative HTE mechanism. For such detached pin-fin channel with the clearance to pin-diameter ratio of 1/4, the reductions in endwall Nusselt number (Nu) arising from the attached pin-fin references are less than 10%; while the pressure drop coefficients in this detached pin-fin channel fall dramatically to the levels about 40% of those in the attached pin-fin channel and result in the improvements in thermal performance factors [16]. However, when occasions demand for further endwall HTE performances in a pin-fin channel, the combination of other HTE measure(s) with pin-fin array to form the so-called compound HTE device is required. It is worth noting that, unlike the channel enhanced by angled ribs which induce strong cross-plane secondary flows as a major HTE mechanism; these pin-fins can disrupt such rib-induced secondary flows considerably. It is therefore considered to combine the pin-fin array with the deepened scales [17] in order to merge the HTE mechanisms triggered by the pin-fin array and the scale imprints.

With scaled imprints over an enhanced channel wall, the boundary layers are repeatedly broken with the intensified turbulence. Taking the fin effects into account, Nusselt number ratios (Nu/Nu_∞) for a scale-roughened narrow channel can reach about 3 and 4.5 for the backward and forward turbulent flows, respectively [17]. Our recent flow measurements [18] disclose the flow physics associated with such HTE impacts inside a rectangular channel with two opposite walls roughened by deepened scales. In the spanwise direction, each deepened scale triggers a jet-like central flow with a pair of counter-rotating vortices on its two sides complying within the scale. The near-wall counter-rotating vortex pairs serve as the essential HTE mechanism. These vortex pairs roll the heated fluids toward the core region from the wall by the vortex array functioning as the roller and are subsequently convected downstream to merge with the main stream. Above the near-wall vortex array, the unstable and transient large-scale vortices are visualized which affect the turbulent structures. The roller-like vortex arrays, dominant streamwise convective velocities, and the higher turbulent kinetic energy levels are concluded as the main HTE mechanisms for the scale-roughened channel with forward flows [18]. As these secondary vortices are absent for the downward flows, forward flow cases consistently provide higher HTE effects than their downward flow counterparts in scale-roughened channels.

Driven by the needs to further elevate endwall HTE impacts for the pin-fin channel with cooling applications to gas turbine blades and electronic chipsets, the compound HTE measure is devised by combining the deepened surface scales and the pin-fin array. The present experimental study comparatively examines the HTE ratios, pressure drop characteristics and thermal performance factors for roughened pin-fin channels. No previous study is available for this novel compound HTE measure which merges the complex flow features induced by the pin-fin array and the scale imprints over the endwalls.

2. Experimental details

2.1. Test facilities

Fig. 1 depicts (a) schematics of the experimental facility and (b) the pin-fin array and scale-roughened surface. As shown in Fig. 1a, the screw-type compressor (1) and the refrigerating unit (2) supplied the dehumidified and cooled airflow to the test assembly at the ambient temperature level. The test airflow was channeled through a set of pressure regulator and filter (3), a needle valve (4), a mass flow meter (5) and a pressure transducer (6) through which the pressure and the mass flow rate of the test coolant entering the

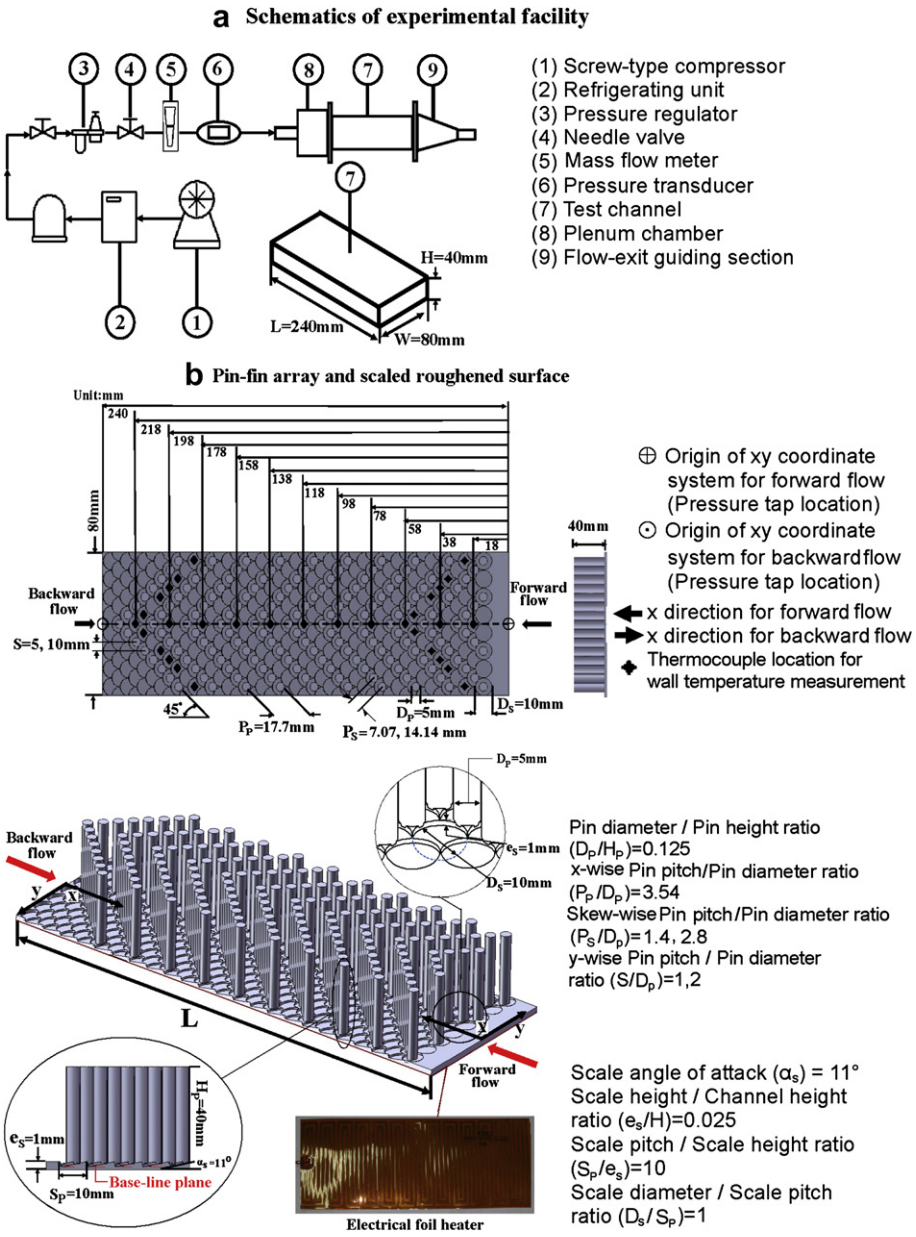

Fig. 1. Experimental test facility.

pin-fin test channel (7) was adjusted and measured. The pin-fin test channel (7) was 240 mm × 80mm × 40 mm in dimension with two opposite walls roughened by deepened scales. The aspect ratio (H/W) and the hydraulic diameter of the rectangular test channel were 1/2 and 53 mm, respectively. The pressurized airflow was fed into a 240 mm × 80mm × 80 mm plenum chamber (8) prior to entering the test channel. The cross-sectional area ratio between the plenum chamber and the test channel was 2 that simulated the abrupt entry condition. As the electrical heating also commenced at the immediate flow entrance, the hydraulic and thermal boundary layers were developed simultaneously at the flow entrance. A K-type thermocouple penetrated into the core of the plenum chamber adjacent to the entry plane of the test channel to detect the coolant entry temperature which was constantly used to calculate the fluid properties at the flow entrance for evaluating Reynolds (*Re*) and Prandtl (*Pr*) numbers there. The calculation procedure for assessing the fluid bulk temperatures (T_b) at locations corresponding to the axial spots where the wall temperatures (T_w) were measured was conducted using the sequential enthalpy balance method. Three type K thermocouples with equal spanwise interval penetrated into the core of the convergent exit chamber (9) adjacent to the exit plane of the test channel to measure local exit fluid temperatures. The exit fluid temperature was obtained by averaging the three thermocouple measurements and used to compare with the calculated T_b at the channel exit during the stage of data acquisition in order to constantly check the accuracy of energy conservation. Raw data batch was accepted for subsequent data processing when the differences between the measured and calculated T_b at the exit plane of the test channel were less than 8%.

The geometrical details of pin-fin array and the scale-roughened endwalls are depicted in Fig. 1b. As indicated, the surface topologies encountered by the forward and backward flows over the scale-roughened surface are different so that the heat transfer and pressure drop in such a scale-roughened channel depend on the

direction of main flow [17]. The coordinate systems for the forward and backward flows as well as the thermocouple locations for T_w measurements are also indicated in Fig. 1b. To eliminate the additional fin effects provided by the pin-fin array to reveal the actual endwall heat transfer performances, each pin-fin is made of Teflon with thermal conductivity about 0.23 Wm^{-1} K^{-1}. Each Teflon pin with the height (H_P) of 40 mm and 5 mm in diameter (D_P) is positioned at the geometric center of each scale imprint to form the V-shaped in-line pin-fin array characterized by the following geometrical dimensionless groups:

Skewness of V-shape pin-fin array $= 45^0$
Pin diameter-to-height ratio (H_P/D_P) $= 8$
X-wise pin-pitch to pin-diameter ratio (P_P/H_P) $= 3.54$
Skew-wise pin pitch-to-diameter ratio (P_S/H_P) $= 1.4$ or 2.8
Y-wise pin pitch-to-diameter ratio (S/H_P) $= 1$ or 2

Endwall heat transfer performances and pressure drop characteristics for the scale-roughened pin-fin channels are examined for two pin-fin arrays with different y-wise (skew-wise) pin pitch-to-diameter ratios of 1 and 2 (1.4 and 2.8). As shown in Fig. 1-b, the coherent scale imprints are arranged in the staggered manner and deepened into two opposite channel wide walls characterized by four dimensionless geometrical groups of:

Scale angle of penetration (α_S) $= 11^0$
Scale height to channel height ratio (e_S/H) $= 0.025$
Scale pitch-to-height ratio (S_P/e_S) $= 10$
Scale diameter to scale pitch ratio (D_S/S_P) $= 1$

Each scale-roughened surface was machined from the stainless steel plate with the thermal conductivity of 15 Wm^{-1} K^{-1} and electrically heated by a 0.5 mm thick Minco thermal foil. The heating foil was sandwiched between a 25 mm thick Teflon plate and the stainless steel made heat transfer surface which generated the basically uniform heat flux heating condition.

Eleven streamwise K-type thermocouples with equal interval of 20 mm were installed on the back face of the scale-roughened wall along the centerline for T_w measurements. Each centerline thermocouple measuring T_w located precisely at the midway between two x-wise adjacent pins irrespective to the forward and backward flow conditions. A further ten thermocouples were installed symmetrically to the centerline in the skew-wise direction between two adjacent V pin-rows at two ends of the scale-roughened surface, as indicated in Fig. 1b. Local Nu derived from each set of eleven T_w measurements in the skew-wise direction between the two V pin-rows are averaged to give the averaged $Nu(\overline{Nu})$ featuring the endwall heat transfer level in the developed flow region for forward or backward flows. Re and Nu were experimentally defined as:

$$Re = \rho W_m d/\mu \quad (1)$$

$$Nu = qd/[k_f(T_w - T_b)] \quad (2)$$

where ρ, W_m, d and μ are the fluid density, bulk mean flow velocity, hydraulic diameter of test channel and viscosity of fluid respectively. k_f, T_w and T_b in equation (1) are the thermal conductivity of coolant, the wall temperature evaluated at the wall-to-fluid interface and the local fluid bulk temperature determined from the enthalpy balance method. All the fluid properties required to calculate Re and local Nu were evaluated from the local fluid bulk temperature (T_b).

The local convective heat flux (q) for Nu evaluation was obtained by subtracting the local heat loss flux from the supplied heat flux over the electrical heating foil. The heating surface adopted to evaluate the heat fluxes included all surfaces of the scale imprints. The area ratio between the present scale-roughened surface and the base-line plane indicated in Fig. 1b is 1.4. To minimize the external heat loss from the heated test section, layers of thermal insulation material were wrapped over the outer surface of the test channel. The characteristic of such external heat loss was examined through a series of heat loss calibration tests which revealed the proportionality between the heat loss flux and the wall-to-ambient temperature difference. The correlation for estimating the heat loss flux was accordingly derived and built into the data processing program to determine the local convective heat flux transferred by the flow (q). In this respect, local q varied over the scale-roughened endwall as measured wall temperatures (T_w) were not uniformly distributed due to the location dependent Nu distributions created by the flow. With a uniform heat flux supplied from the Minco thermal foil, the convective heat flux was obtained by subtracting the local heat loss flux from the total heat flux supplied at each location where T_w was detected. The review of the entire post-processed q data indicated the maximum non-uniformity in heat flux distributions of 8.3% due to the small amount of external heat loss.

All the temperature measurements were monitored and stored in PC through a Fluke Hydra 2640 A data logger. T_w measurements were corrected into the base-line plane as indicated in Fig. 1-b using the one dimensional heat conduction equation. Origins of streamwise (x) and spanwise (y) coordinate systems for the forward and backward flows were selected at the middle span of each entry edge.

Pressure drop tests were carried out separately at isothermal conditions. At each Re tested, the pressure differences across the entire test channel in terms of mm-H_2O were detected through two flexible tubes connected with the pressure taps of 0.5 mm diameter at two origins of the coordinate systems specified in Fig. 1b. Pressure differences between these two taps were measured by a digital micromanometer with precision of 0.001 mm-H_2O. Such arrangement for pressure drop measurements offered the overall assessments for the flow resistance over the entire test channel, which generated the higher pressure drop coefficients than those acquired from the developed flow regime. The dimensionless pressure drop over the test channel was evaluated as the Fanning friction factors (f) based on the pressure drops (ΔP) across the test channel of length L with mean flow velocity (W_m) as:

$$f = \left[\Delta p/\left(0.5\rho W_m^2\right)\right](d/4L) \quad (3)$$

2.2. Procedures and data processing

Heat transfer and pressure drop tests were individually performed with the airflows directed in forward and backward directions at Re = 1000, 1500, 2000, 5000, 10 000, 15 000, 20 000, 25 000, 30 000. Streamwise centerline Nu distributions along the scale-roughened endwall, $\overline{Nu}$ and pressure drop coefficients (f) in the tested Re range, which covered both laminar and turbulent flows, were examined. The inclination angles of these scale imprints are unidirectional and the V pin-rows were pointed in the downstream (upstream) direction for the forward (backward) flows, the performances of heat transfer and pressure drop in the present test channel were affected by the direction of main flow. Therefore the Re impacts on local Nu, $\overline{Nu}$, pressure drop coefficients and thermal performance factors for forward and backward flows are individually examined. The HTE ratios in terms of $\overline{Nu}/Nu_\infty$ along with the penalty of augmentations in pressure drops and the thermal performance factors between the present test channel and those collected from a variety of enhanced channels were

compared. A set of empirical correlations that evaluated $\overline{Nu}$ and f for the present test channel with forward and backward flows were generated to assist engineering applications.

This experimental program performed the steady state heat transfer tests. The steady state was assumed when the T_w variations with several successive scans at one detected location were less than 0.3 °C. The elapsed time to satisfy such steady state assumption generally took 30–45 min after the heating power or the airflow rate was adjusted. It is worth noting that the various heat fluxes fed into the test channel affected *Re* at the flow entrance even if the airflow rate remained invariant due to the thermal impacts on the fluid properties. Adequate adjustments of airflow rate to compensate the variations in fluid properties due to heat transfer were constantly performed to keep the maximum differences in *Re* at the entry plane of the test channel within ±1% from the targeting value.

The references selected to assess HTE ratios and pressure drop augmentations in the present scale-roughened pin-fin channel were those developed in a smooth-walled circular tube with fully developed flow. The referenced Nusselt number (Nu_∞) and pressure drop coefficient (f_∞) for laminar and turbulent flows are defined in equations (4)–(7).

$$Nu_\infty = 48/11 \quad \text{(laminar pipe flow with uniform heat flux)} \tag{4}$$

$$f_\infty = 16/Re \quad \text{(laminar pipe flow)} \tag{5}$$

$$Nu_\infty = 0.023Re^{0.8}Pr^{0.4} \quad \text{(Dittus-Boelter correlation for turbulent flow)} \tag{6}$$

$$f_\infty = 0.079Re^{-0.25} \quad \text{(Blasius equation for turbulent pipe flow)} \tag{7}$$

The thermal performance factor (η) based on the constant pumping power consumption is quantified as:

$$\eta = (\overline{Nu}/Nu_\infty)/(f/f_\infty)^{1/3} \tag{8}$$

The temperature measurements were the major sources for the uncertainties in *Nu* and *Re* as the properties of coolant such as thermal conductivity and viscosity were evaluated in accordance with the local fluid bulk temperature. Based on the precisions provided by the measurement devices, the maximum uncertainties of the derived parameters for constituting the governing dimensionless groups are estimated as: heat flux (0.8%), fluid viscosity (0.35%), fluid thermal conductivity (0.28%) and fluid specific heat (0.01%). The maximum uncertainties associated with *Nu, Re* and *f* were respectively estimated as 9.6% and 5.8% and 3.1% following the policy of ASME on reporting the uncertainties in experimental measurements and results [19].

3. Results and discussion

3.1. Nu measurements and $\overline{Nu}$ correlations

Fig. 2 compares the streamwise centerline *Nu* distributions along the scale-roughened endwall with pin-fin arrays of $S/D_P = 1, 2$ between forward and backward flows at *Re* = 1000, 5000, 10 000, 20 000, 30 000. The *Nu* levels in each scale-roughened pin-fin channel are systematically elevated by increasing *Re* from 1000 to 30 000; while the pin-fin array with $S/D_P = 1$ consistently contribute to the higher *Nu* than the counterparts obtained with $S/D_P = 2$. Unlike the pattern of streamwise *Nu* increase found in a pin-fin channel with smooth endwalls [16], each *Re* controlled *Nu* variation depicted in Fig. 2 follows a general trend of exponential decay similar to that developed in the scale-roughened channel without pin-fin array [17]. For a pin-fin channel with smooth endwalls, the trade-offs between two rival mechanisms, namely the streamwise growth of HTE impacts triggered by pin-rows and the thickened downstream boundary layers, generate the overall streamwise *Nu* increase accompanying by the pin-tripped *Nu* ripples [16]. Although the horseshoe vortices tripped at each pin-endwall junction remain persistent in the present scale-roughened pin-fin channel, the vortical structures induced by the scale imprints [18] in the present test channel play the dominant role for surface heat transfer so that the streamwise centerline *Nu* distributions collected in Fig. 2 follow the typical patterns resolved in the scale-roughened channel without pin-fin array [17]. Due to the dominant heat transfer features generated by the scale imprints, the abrupt entrance effects elevate *Nu* levels in the developing flow region over the axial spans about $0 < x/d < 2.5$ and $0 < x/d < 3$ for the forward and backward flows respectively. As seen in Fig. 2, the flow reaches the developed region after about 8th pin-row for the present scale-roughened pin-fin channel. In the pin-fin channels with smooth endwalls [13,16], the developing length is about 4–5 pin-rows. The present scale-roughened pin-fin channel requires the longer developing length than that in a smooth-walled pin-fin channel. Clearly, the increased developing length for the present test channel from the smooth-walled pin-fin channel is indicative of the longer settling length for the flow interactions between the vortices tripped by the scale imprints and the pin-rows. At the exit end of the present test channel, *Nu* elevations over the final 15% of the heat sink for both forward and backward flows are observed in Fig. 2, due to the end loss effect. In the axial region affected by the end heat loss, the wall temperature distribution drops in the axial direction due to the conductive heat loss toward the supporting parts that connect with the exit end of the heated test channel; while the flow field has reached the developed regime. Therefore the *Nu* data collected from the final 15% of the heat sink for both forward and backward flows are discarded when the averaged *Nu* over the developed flow region is evaluated.

It is worth noting that, as each thermocouple is positioned exactly at the midway between two adjacent pin-rows, there is no sign of pin-row driven *Nu* ripples displayed in Fig. 2. But the direction of main flow has profound influences on endwall *Nu* levels for the present test channels with pin-fin arrays. As compared in each plot of Fig. 2, the forward flow case consistently shows the higher *Nu* than the backward flow case. Such *Nu* differences between forward and backward flows are resulted from the subtle differences in flow structures between the forward and backward flows over the scale imprints [17,18] even if the agitated vortical flows tripped by pin-rows prevail over the entire pin-fin test channel. With forward flows over the present scale-roughened surface, the near-wall vortex array plays a significant role for HTE impacts. As such near-wall vortex array and its associated unstable, transient large-scale vortices in the scale-roughened channel with forward flows are absent in a similar channel with backward flows [18], the forward flow cases consistently provide higher HTE effects than the backward flow counterparts in the scale-roughened channel [17,18] as well as in the present scale-roughened pin-fin channel. In this respect for the scale-roughened channel with two pin-fin arrays of $S/D_P = 1$ and 2, the larger degrees of such forward-to-backward *Nu* differences, which increase as *Re* increases, develop in the pin-fin channel with $S/D_P = 1$. This particular result indicates that the flow interactions between the vortical flows triggered by pin-fin arrays and scales are different between the forward and backward flows. But these pin-fins and the scale imprints are unlikely to induce the strong cross-plane secondary flows which play the dominant roles for HTE impacts in

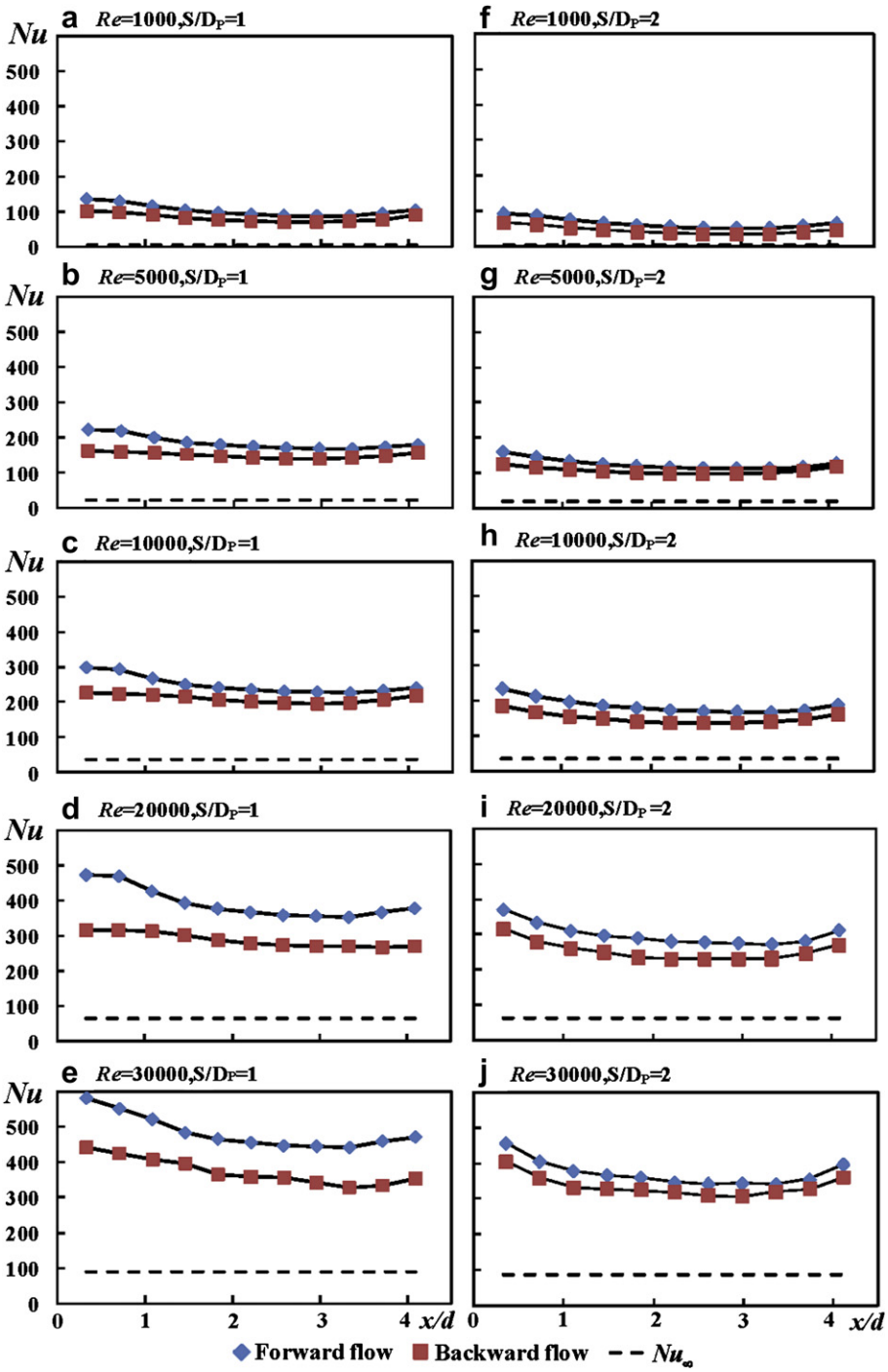

Fig. 2. Centerline *Nu* variations on scale-roughened endwall with two pin-fin arrays of $S/D_P = 1$ and 2 at $Re = 1000$, 5000, 10,000, 20,000, 30,000.

the channels roughened by angled ribs. Due to the lack of strong secondary flows over the cross section of the present scale-roughened pin-fin channel in the developed flow regions between pin-rows 10–11 and 9–10 for the forward and backward flows respectively, the *Nu* variations along y/W axis as depicted by Fig. 3 are quite uniform. Nevertheless, the *Nu* values at locations aside $y/W = \pm 0.5$ in each plot of Fig. 3 are slightly reduced from those in the central region due to the thickened boundary layers developed over two channel sidewalls, which has been previously reported for the rectangular channel with attached pin-fin arrays [16]. Therefore the considerable heat transfer elevations from the Nu_∞ references as compared in each plot of Fig. 2 are generated by the compound mechanisms including the boundary layer breaking, the near-wall vortices, the enhanced turbulence and the vortical structures evolved from the horseshoe vortices. Nevertheless, as each skew-wise thermocouple locates precisely at the midway between two adjacent V pin-rows, there is no y-wise *Nu* ripple shown in Fig. 3. By way of averaging each y-wise *Nu* profile depicted in Fig. 2 resolves into $\overline{Nu}$ representing the averaged heat transfer level in the developed flow region at midway locations behind the pin-row.

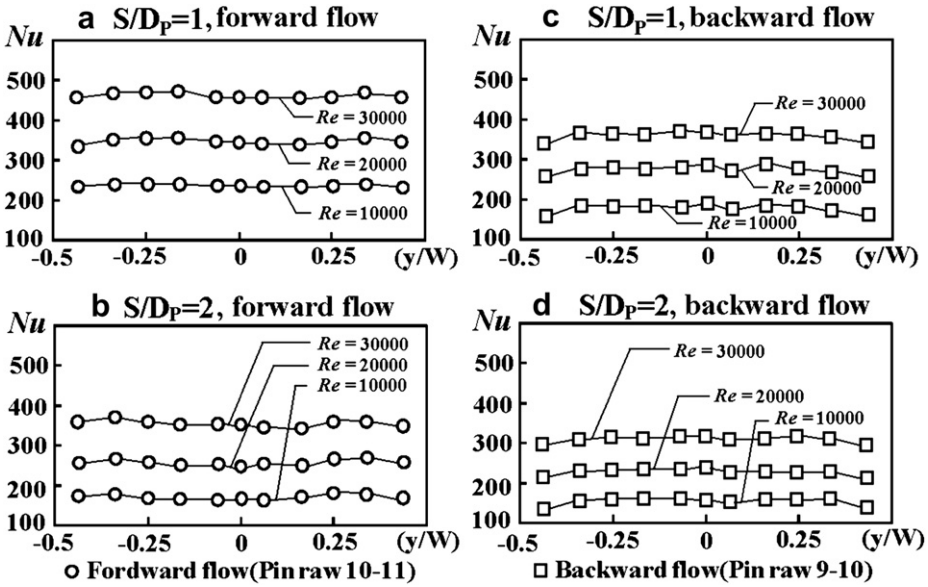

Fig. 3. Spanwise *Nu* variations with pin-fin arrays of (a) $S/D_P = 1$, forward flow (b) $S/D_P = 2$, forward flow (c) $S/D_P = 1$, backward flow (d) $S/D_P = 2$, backward flow at $Re = 10{,}000$, 20,000, 30,000.

Fig. 4 depicts the varying trends of $\overline{Nu}$ versus *Re* for forward and backward flows with pin-fin arrays of $S/D_P = 1$ and 2. The referenced Nusselt numbers (Nu_∞) for laminar and turbulent flows over the tested *Re* range are indicated as the dotted line in Fig. 4 for comparisons. As compared in Fig. 4, the $\overline{Nu}$ obtained with forward flows consistently operate at the higher levels than their backward-flow counterparts; while the $\overline{Nu}$ obtained with the pin-fin array of $S/D_P = 1$ are higher than those obtained with $S/D_P = 2$ for forward or backward flows. All the *Re*-driven $\overline{Nu}$ trends displayed in Fig. 4 can be well correlated as $\overline{Nu} = A \times Re^n$ in which the A coefficient and *n* exponent vary with the main flow direction and S/D_P. The mathematical form of correlation satisfies the limiting condition of vanished forced convective capability ($\overline{Nu} \to 0$) as $Re \to 0$. Table 1 compares the A, *n* values collected from the various $\overline{Nu}$ correlations derived from the present test channel, the smooth-walled pin-fin channel [16], the scale-roughened channel [17] and the channel with the compound V-ribs and scales [20]. Among this comparative group, the geometries of surface scales and the channel aspect ratios (AR) for the scale-roughened channel [17], the present test channel and the channel with compound V-ribs and scales [20] are identical so that these results can be compared directly to reveal the impacts of the additional V-ribs and present pin-fin arrays on A, *n* coefficients. However, for the pin-fin channel with smooth endwalls [16], the channel aspect ratio is 4 and the x-wise and y-wise pin pitch-to-diameter ratios for the in-line array are 2. As this study is the first time attempt to arrange the V-shaped pin-fin array, no direct relevant $\overline{Nu}$ data is available for such comparison and the results obtained from the pin-fin channel with smooth endwalls [16] mainly serve as references to examine the impacts of scale imprints on *n* exponents.

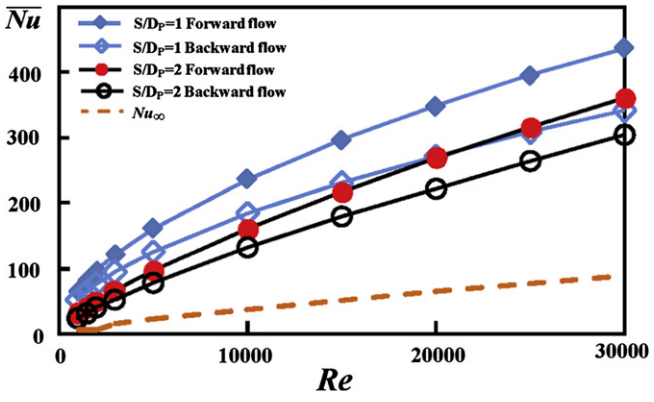

Fig. 4. Comparisons of $\overline{Nu}$ versus *Re* between forward and backward flows with pin-fin arrays of $S/D_P = 1$ and 2.

As shown in Table 1, the present scale imprints fitted into the plain channel [17] or combined with V-ribs [20] and the present pin-fin array consistently raise the *n* exponents (of the dependence on Reynolds' number) from the similar channels without scale imprints. With $S/D_P = 2$, the *n* exponents in $\overline{Nu}$ correlations for the present scale-roughened pin-fin channel as indicated in Table 1 are respectively raised to 0.737 and 0.764 for the forward and backward flows from the reference value of 0.6 for the pin-fin channel with smooth endwalls [16]. Similarly for the ribbed channels, the *n* exponents in $\overline{Nu}$ correlations for the scale-roughened channel with V-ribs are respectively raised to 0.787 and 0.649 for the forward and backward flows from the typical value of 0.6 for the rib-roughened channels [21–23]. In general, the *Re* exponent (*n* value) in Nu_∞ correlation for a smooth-walled channel with turbulent flow is 0.8. The increase of *n* exponent in $\overline{Nu}$ correlation toward or above 0.8 can extend the effective *Re* range with HTE impact ($\overline{Nu}/Nu_\infty > 1$). Another interesting feature disclosed by Table 1 is the increased *n* exponents as S/D_P increases from 1 to 2 for the present test channels. A physical interpretation of this result is the reduced *Re* range for HTE impacts as S/D_P decreases from 2 to 1 even if the present $\overline{Nu}$ with $S/D_P = 1$ still remain higher than those obtained with $S/D_P = 2$ in the *Re* range of 1000–30000. By way of intensifying the density of pin-fin array enhances the dominance of heat transfer characteristics initiated by the horseshoe vortices so that the heat transfer impacts due to the flow structures tripped by the scale imprints [18] are relatively weakened. As the dominance of scale-driven flow phenomena on heat transfer performances is weakened by intensifying the density of pin-fin array, the differences in *n* exponents between forward and backward flows for the

Table 1
Comparison of A coefficient and n exponent in $\overline{Nu} = A \times Re^n$ correlations for various HTE measures in rectangular channels.

HTE measure	Coefficient A				Exponent n			
	Scale + Pin-fin array	Scale	Pin-fin array	Scale + V-ribs	Scale + Pin-fin array	Scale	Pin-fin array	Scale + V-ribs
$S/D_P = 1$, forward flow	1.36	0.09		0.16	0.56	0.82		0.79
$S/D_P = 1$, backward flow	1.05	0.17		0.49	0.56	0.7		0.65
$S/D_P = 2$, forward flow	0.18	0.09	0.51	0.16	0.74	0.82	0.6	0.79
$S/D_P = 2$, backward flow	0.12	0.17	0.51	0.49	0.76	0.7	0.6	0.65

present test channel with $S/D_P = 1$ are reduced from those obtained with $S/D_P = 2$ as compared in Table 1. As a result, the beneficial HTE performances attributing from the scale imprints, such as the extension of the effective *Re* range with HTE impacts, are weakened when the pin pitch-to-diameter ratios are reduced. However, the *Re* exponents of 0.737 and 0.764 for the present scale-roughened pin-fin channel with $S/D_P = 2$ are both elevated from the typical value of 0.6 for the pin-fin channels with smooth endwalls and approach 0.8 in the Dittus-Boelter correlation. Thus the effective *Re* range within which $\overline{Nu}/Nu_\infty > 1$ can be extended by combining the scale imprints with the pin-fin array. This is particularly useful for turbine blade cooling applications as the practical *Re* for internal coolant channels are often higher 30 000. Nevertheless, for the present test channels with $1000 \le Re \le 30\,000$, 95% of the experimental $\overline{Nu}$ data agree within ±10% discrepancies from the results calculated by the correlations. It is worth noting that, as *Pr* effects are absorbed into the coefficients in $\overline{Nu}$ correlations, which are not included as a parametric effect when these correlations are developed here, the four $\overline{Nu}$ correlations derived for the present test channels are essentially limited to dry air.

The HTE impacts of present scale-roughened pin-fin channels are evaluated as the Nusselt number ratios in terms of $\overline{Nu}/Nu_\infty$. Although each *Re*-driven $\overline{Nu}$ variation showed in Fig. 4 is followed by the continuously monotonic increase, two different patterns of $\overline{Nu}/Nu_\infty$ versus *Re* for laminar and turbulent flows are resolved in Fig. 5 due to the different Nu_∞ references selected for laminar and turbulent flows. Also compared in Fig. 5 are the $\overline{Nu}/Nu_\infty$ ratios reported from different research groups using various HTE devices [21–23]. With $Re \le 2000$, $\overline{Nu}/Nu_\infty$ for the present scale-roughened pin-fin channels with forward and backward flows respectively fall in the ranges of 14.9–22 and 11.6–17.1 with $S/D_P = 1$ and 6.7–11.2 and 5.2–8.7 with $S/D_P = 2$. As Nu_∞ remains as 48/11 in the *Re* range of 1000–2000, all the $\overline{Nu}/Nu_\infty$ trends obtained from the channels fitted with various HTE devices increase as *Re* increases as seen in Fig. 5. However, as Nu_∞ is proportional to $Re^{0.8}$ for developed turbulent flows in the *Re* range of 3000–30000, the $\overline{Nu}/Nu_\infty$ ratios

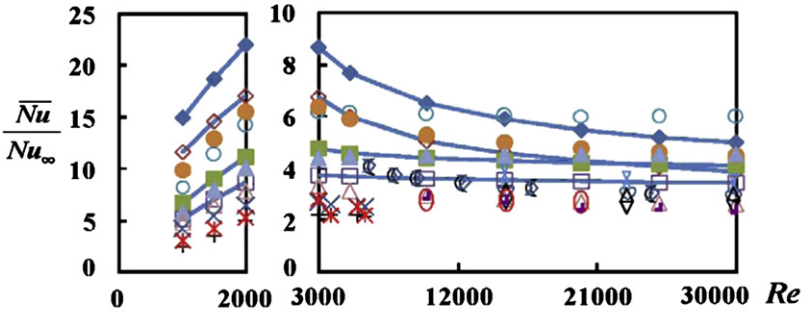

	References	AR	α^R	Pitch ratio	e/H	HTE device	EAR
◆	Forward flow S/D_P=1 (present study)	2	45	10	1	Pin fins Scaled surface	8.85
◇	Backward flow S/D_P=1 (present study)	2	45	10	1	Pin fins Scaled surface	8.85
■	Forward flow S/D_P=2 (present study)	2	45	10	1	Pin fins Scaled surface	5.88
□	Backward flow S/D_P=2 (present study)	2	45	10	1	Pin fins Scaled surface	5.88
⧖	Han et al. 45deg V-up rib[21]	1	45	10	0.0625	Continuous rib	1.67
♡	Han et al. 45deg V-Down rib[21]	1	45	10	0.0625	Continuous rib	1.67
⧖	Han et al. 45deg angled rib [21]	1	45	10	0.0625	Continuous rib	1.7
☾	Taslim et al. 45deg angled rib [22]	1	45	10	0.083	Continuous rib	2.19
»	Taslim et al. V Discrete rib [22]	1	45	10	0.083	Discrete rib	2.19
+	Gao & Sunden 60deg V-up rib [23]	8	60	10	0.1	Continuous rib	1.85
×	Gao & Sunden 60deg V-down rib [23]	8	60	10	0.1	Continuous rib	1.85
✱	Gao & Sunden 60deg angled rib [23]	8	60	10	0.1	Continuous rib	1.69
▲	Chang et al. forward flow [17]	8		10	0.1	Scaled surface	2.27
△	Chang et al. backward flow [17]	8		10	0.1	Scaled surface	2.27
○	Chang et al. forward flow[20]	2	45	10	0.044	V-rib Scaled surface	2.43
●	Chang et al. backward flow[20]	2	45	10	0.044	V-rib Scaled surface	2.43
▪	Chang et al. [16]					In-line pin-fin array	2.8
0	Chyu et al.[24]					In-line pin-fin array	3.96

Pitch ratio referred in this table is for surface ribs and scales.

Fig. 5. Comparison of $\overline{Nu}/Nu_\infty$ ratios between various HTE devices.

collected in Fig. 5 for the channels with various HTE devices generally decrease with the increase of *Re* to reflect the correlation results of $n < 0.8$ for the most of passive HTE devices in channels. With $3000 \leq Re \leq 30\,000$, the $\overline{Nu}/Nu_\infty$ for the present scale-roughened pin-fin channels with forward and backward flows reach the levels of 8.6–4.98 and 6.7–3.9 with $S/D_P = 1$ and 4.8–4.1 and 3.7–3.4 with $S/D_P = 2$. For the present test channels, the descending rates of $\overline{Nu}/Nu_\infty$ against *Re* with $S/D_P = 1$ are faster than those with $S/D_P = 2$ and than those with compound scales and V-ribs [20]. As a result, $\overline{Nu}/Nu_\infty$ for the channel with compound roughness of scales and V-ribs [20] turn to be higher than the $\overline{Nu}/Nu_\infty$ levels in the present pin-fin channel with $S/D_P = 1$ when *Re* exceeds 20 000. With the compound roughness of scales and V-ribs, the V-ribs induce strong cross-sectional secondary flows swirling along the entire channel. While the turbulent eddies induced by the scale imprints [18] are interacting with the secondary flows induced by the V-ribs among the channel core, the near-wall vortex array and the turbulence augmentation [18] can still prevail over the scaled wall to considerably augment HTE impacts. But with the presence of pin-fin array, the near-wall vortex array induced by the scale imprints is constantly distributed by the protruding pin-fins. The strong secondary flows induced by the V-ribs are absent in the present test channel. As a result, the $\overline{Nu}/Nu_\infty$ for the channel with compound roughness of scales and V-ribs are higher than those for the present study at $S/D_P = 1$ and *Re* exceeds 20 000. Nevertheless, even with $S/D_P = 2$ for the present test channel, the $\overline{Nu}/Nu_\infty$ ratios indicated in Fig. 5 still exceed the $\overline{Nu}/Nu_\infty$ ratios in the rib-roughened channels [21–23]. Particularly, while the $\overline{Nu}/Nu_\infty$ for the smooth-walled pin-fin channels remain in the ranges of 1.8–2.5 [14,16] as seen in Fig. 5, the present scale-roughened pin-fin channels significantly enhance the HTE impacts by elevating the $\overline{Nu}/Nu_\infty$ ratios to 5.16–22 in the *Re* range of 1000–30000. The augmentations of HTE impacts by incorporating the scale imprints over the endwalls of the pin-fin channels are remarkable.

The increased heat transfer area from the base-line plane by a pin-fin array is significant. This is evaluated as the Effective Area Ratio (EAR) in Fig. 5 for each HTE device as the area ratio between the total convective surfaces to the base-plane area. As compared in Fig. 5, while the EAR for the ribbed or scale-roughened channels scatter between 1.6 and 2.5, the EAR for the present pin-fin channels with $S/D_P = 1$ and 2 reach 8.85 and 5.88 respectively. In view of the heat transfer powers by taking EAR into account for comparing the thermal performances offered by the various HTE measures, the high EAR for the pin-fin array can offset the increased pressure-drop penalties which will be demonstrated later in the paper.

3.2. *f* measurements and correlations

Fig. 6a and b respectively depict *f* versus *Re* for the present scale-roughened pin-fin channels with (a) $S/D_P = 1$ and (b) $S/D_P = 2$. Also compared in Fig. 6b are the experimental data collected from the pin-fin channels with pin pitch-to-diameter ratios of 2 in both × and y directions [16,24]. It is worth noting that, for both present scale-roughened pin-fin channels, the x-wise pin pitch-to-diameter ratio (P_P/D_P) is fixed at 3.54 which is larger than the P_P/D_P ratio of 2 used by [16,24]. But, as compared in Fig. 6-b, the *f* factors for the present test channel with $S/D_P = 2$, $P_P/D_P = 3.54$ are higher than the *f* values detected from the smooth-walled pin-fin channels with $S/D_P = 2$, $P_P/D_P = 2$ [16,24] due to the presence of scale imprints. It is clear that the most of pressure drop in the present scale-roughened pin-fin channels arises from the flow resistance through the pin-fin array rather than the scale imprints. This conclusion can be justified by the small *f* difference between the present data and those reported in [16,24] as compared in

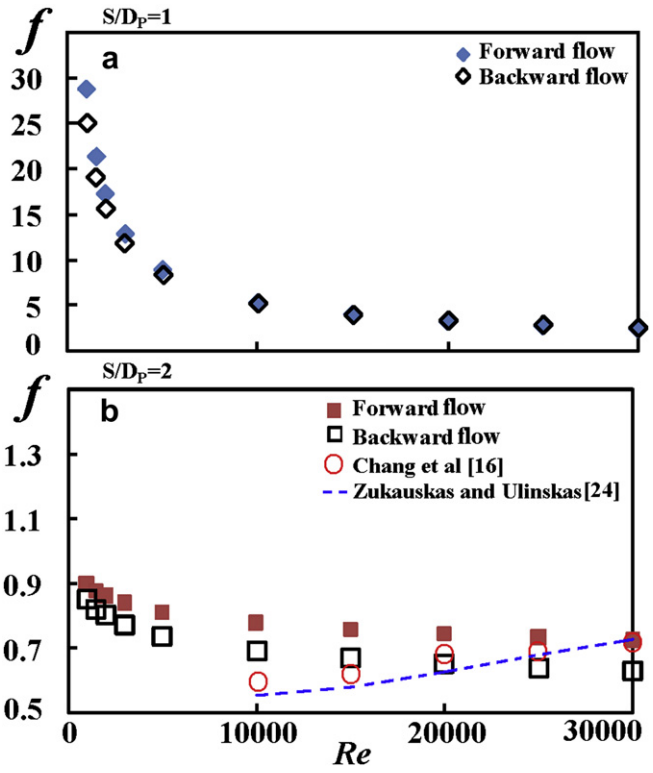

Fig. 6. *f* versus *Re* for scale-roughened pin-fin channels with (a) $S/D_P = 1$ and (b) $S/D_P = 2$.

Fig. 6-b. The large pressure drop through a pin-fin channel has always been the major drawback for such HTE device. When the dominance of horseshoe vortices is enhanced by intensifying the density of pin-fin array as demonstrated by the previous heat transfer results, it is interesting to note that the differences in *f* factor between the forward and backward flows in the present test channel with $S/D_P = 1$ tend to be diminished as seen in Fig. 6a. By way of increasing S/D_P from 1 to 2, the *f* differences between the two comparative cases with forward and backward flows are observed as seen in Fig. 6b. In this respect, the *f* factors with forward flows in the channel of $S/D_P = 2$ constantly operate at the higher levels than the backward-flow counterparts. Clearly, the enhanced scale-driven impacts on the flow interactions between the vortices tripped by scales and pin-rows have led such *f* difference between the cases with forward and backward flows. Irrespective to the aforementioned S/D_P impacts, *f* factors collected in Fig. 6 consistently decrease toward the asymptotic values for both forward and backward flows in both tested channels as *Re* increases. In the range of $1000 \leq Re \leq 30\,000$, *f* factors in each test channel with forward and backward flows are well correlated by the equation of $f = E + F \times e^{-G \times Re}$ where the coefficient *E*, *F* and exponent *G* vary with the main flow direction and S/D_P here. Table 2 summarizes the *E*, *F*, *G* values collected from the various *f* correlations derived from the present test channels.

Table 2
Coefficients *E*, F and exponent G in $f = E + F \times e^{-G \times Re}$ correlations.

	$S/D_P = 1$			$S/D_P = 2$		
	E	*F*	*G*	*E*	*F*	*G*
Forward flow	3.12	36.7	4.24E-4	0.63	9.91	7.04E-4
Backward flow	2.75	29	3.45E-4	0.6	22.4	11.9E-4

The augmentations of pressure drop penalty responding to the HTE impacts provided by the compound scale imprints and pin-fin array as seen in Fig. 5 are examined by normalizing the f data with f_∞. The variations of f/f_∞ against Re for forward and backward flows in present pin-fin channels with $S/D_P = 1, 2$ are depicted in Fig. 7 in which the f/f_∞ data reported by various research groups for various single and compound HTE devices are included for comparison. The f/f_∞ ratios for the present test channel with $S/D_P = 2$ and $P_P/D_P = 3.54$ are close to the results detected from the smooth-walled pin-fin channel with $S/D_P = 2$ and $P_P/D_P = 2$ [16], which scatter about 100 from the typical values about 10 for the rib-roughened channels [21–23]. With $S/D_P = 1$ and $P_P/D_P = 3.54$ for the present test channel, the f/f_∞ ratios are raised even higher to the levels about 1000. The significant HTE impacts over the endwall of the scale-roughened pin-fin channels shown in Fig. 5 are accompanied by very high pressure drop penalty due to the pin-fin array. Relative to the pressure drop incurred by the pin-fin array, the pressure drop in association with the scale imprints becomes minor. It is worth noting that the main contribution for f in present test channel is due to the pin-fin array, not the scaled-roughened endwalls. In view of the pressure drops produced by the pin-fin array, there is no considerable difference between the forward and backward flows. Although f in the scale-roughened channel with the forward flow is higher than the counterpart with backward flow [17], the dominant source for determining f in the present test channel for $S/D_p = 1$, which is the pressure drop caused by the pin-fin array, is rather insensitive to the direction of the main flow. As a result, f for backward and forward flows are very similar for $S/D_p = 1$. When the dominance of pin-fin array in determining f factor is weakened by increasing S/D_p, the influence of main flow direction on f factor due to the different pressure drops over the scale-roughened pin-fin channel with forward and backward flows will gradually emerge. The increased pressure drop penalty by incorporating the scale-roughened endwall into a pin-fin channel only plays the minor role for elevating f. But the roller-like vortex array, the dominant streamwise convective velocity, and the higher turbulent kinetic energy [18] has the considerable HTE impact for the present scale-roughened pin-fin channel. When occasions demand for the pin-fin array to be the HTE measure, such the cooling channel in the trailing edge of a gas turbine blade, the scale-roughened endwalls only attribute minor impacts on augmentation of f/f_∞ but can contribute the considerable HTE effect as illustrated in Fig. 5.

Nevertheless, the high pressure drop penalty inherited from the pin-fin array for the present test channels has led to the necessity for comparing the thermal performance factors (η) between the various HTE measures.

3.3. Thermal performance factors and EAR effects

The significant pressure drops incurred by the pin-fin arrays require design considerations. But the considerable increase of convective area available in a pin-fin channel can elevate the heat transfer power to large extents even if the higher Nu surrounding each pin-fin [3,4] are estimated by the endwall Nu levels. As a conservative measure to determine the performances of heat transfer powers attainable from the channels fitted with various

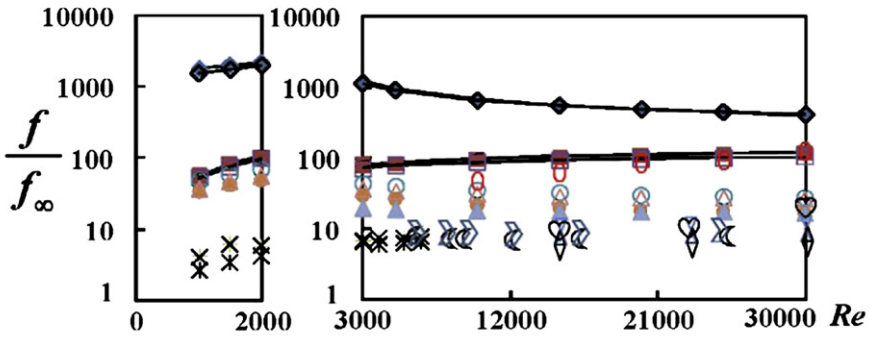

	References	AR	α^R	Pitch ratio	e/H	HTE device	EAR
◆	Forward flow S/D_P=1 (present study)	2	45	10	1	Pin fins Scaled surface	8.85
◇	Backward flow S/D_P=1 (present study)	2	45	10	1	Pin fins Scaled surface	8.85
■	Forward flow S/D_P=2 (present study)	2	45	10	1	Pin fins Scaled surface	5.88
□	Backward flow S/D_P=2 (present study)	2	45	10	1	Pin fins Scaled surface	5.88
⧖	Han et al. 45deg V-up rib[21]	1	45	10	0.0625	Continuous rib	1.67
♡	Han et al. 45deg V-Down rib[21]	1	45	10	0.0625	Continuous rib	1.67
⟠	Han et al. 45deg angled rib [21]	1	45	10	0.0625	Continuous rib	1.7
☾	Taslim et al. 45deg angled rib [22]	1	45	10	0.083	Continuous rib	2.19
»	Taslim et al. V Discrete rib [22]	1	45	10	0.083	Discrete rib	2.19
+	Gao & Sunden 60deg V-up rib [23]	8	60	10	0.1	Continuous rib	1.85
×	Gao & Sunden 60deg V-down rib [23]	8	60	10	0.1	Continuous rib	1.85
✳	Gao & Sunden 60deg angled rib [23]	8	60	10	0.1	Continuous rib	1.69
▲	Chang et al. forward flow [17]	8		10	0.1	Scaled surface	2.27
△	Chang et al. backward flow [17]	8		10	0.1	Scaled surface	2.27
○	Chang et al. forward flow[20]	2	45	10	0.044	V-rib Scaled surface	2.43
●	Chang et al. backward flow[20]	2	45	10	0.044	V-rib Scaled surface	2.43
0	Chang et al. [16]					In-line pin-fin array	2.8

Pitch ratio referred in this table is for surface ribs and scales.

Fig. 7. Comparison of f/f_∞ ratios between various HTE devices.

HTE devices, $\overline{Nu}$ is multiplied by EAR to index the convective capability in terms of the transferred thermal power. From this viewpoint, the thermal performances for various HTE devices are evaluated as $\eta \times$ EAR. Fig. 8 depicts (a) η (b) $\eta \times$ EAR versus *Re* for various HTE devices, which compares the two types of thermal performance factors between a variety of single and compound HTE measures. As compared in Fig. 8-a, the η values for the present test channel with $S/D_P = 2$ are consistently higher than those detected from the test channel with $P_P/D_P = 1$ due to the lower f/f_∞ ratios for both forward and backward flows. Although the $\overline{Nu}/Nu_\infty$ ratios for the present test channels soar among the highest levels in Fig. 5, the significant augmentations in f/f_∞ due to pin-fin arrays have considerably suppressed their thermal performance factors (η) and bring the present test channels down to the lowest values among the comparative group collected in Fig. 8. The highest η values emerge for the channel with compound scales and V-ribs [20] as seen in Fig. 8. With the exception of the channels enhanced by the scale imprints [17] and the compound scales and V-ribs [20], the thermal performance factors (η) for the present test channels as well as the rib-roughened channels [21–23] decrease as *Re* increases for

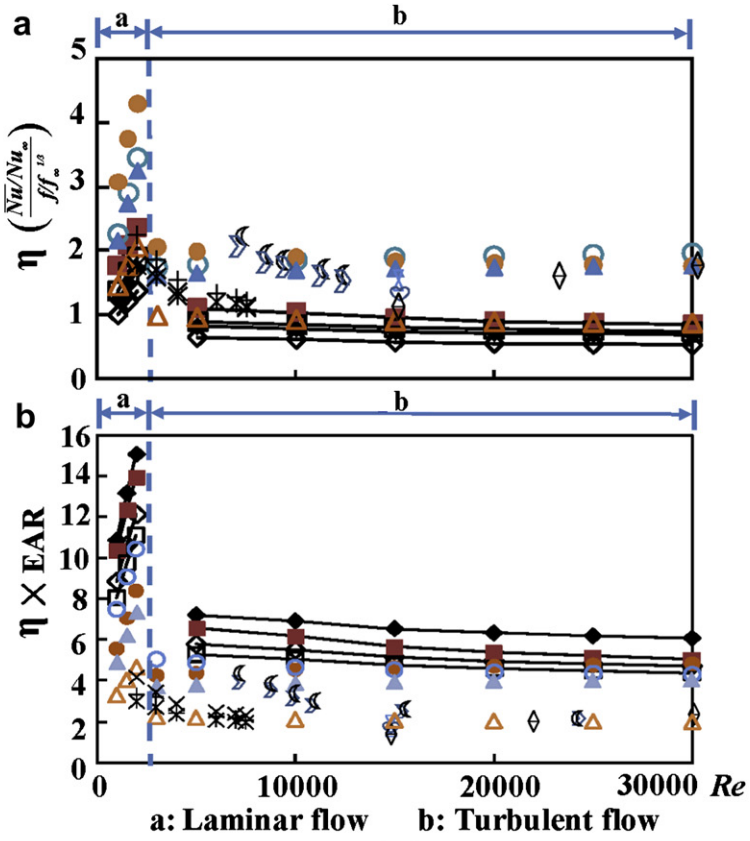

	References	AR	α^R	Pitch ratio	e/H	HTE device	EAR
◆	Forward flow S/D$_P$=1 (present study)	2	45	10	1	Pin fins Scaled surface	8.85
◇	Backward flow S/D$_P$=1 (present study)	2	45	10	1	Pin fins Scaled surface	8.85
■	Forward flow S/D$_P$=2 (present study)	2	45	10	1	Pin fins Scaled surface	5.88
□	Backward flow S/D$_P$=2 (present study)	2	45	10	1	Pin fins Scaled surface	5.88
⧖	Han et al. 45deg V-up rib[21]	1	45	10	0.0625	Continuous rib	1.67
♡	Han et al. 45deg V-Down rib[21]	1	45	10	0.0625	Continuous rib	1.67
◊	Han et al. 45deg angled rib [21]	1	45	10	0.0625	Continuous rib	1.7
☾	Taslim et al. 45deg angled rib [22]	1	45	10	0.083	Continuous rib	2.19
»	Taslim et al. V Discrete rib [22]	1	45	10	0.083	Discrete rib	2.19
+	Gao & Sunden 60deg V-up rib [23]	8	60	10	0.1	Continuous rib	1.85
×	Gao & Sunden 60deg V-down rib [23]	8	60	10	0.1	Continuous rib	1.85
✳	Gao & Sunden 60deg angled rib [23]	8	60	10	0.1	Continuous rib	1.69
▲	Chang et al. forward flow [17]	8		10	0.1	Scaled surface	2.27
△	Chang et al. backward flow [17]	8		10	0.1	Scaled surface	2.27
○	Chang et al. forward flow[20]	2	45	10	0.044	V-rib Scaled surface	2.43
●	Chang et al. backward flow[20]	2	45	10	0.044	V-rib Scaled surface	2.43

Pitch ratio referred in this table is for surface ribs and scales.

Fig. 8. Comparison of (a) η (b) $\eta \times$ EAR versus *Re* between various HTE devices.

turbulent flows. Having considered the increased convective areas from the various HTE devices on their thermal performances, the present scale-roughened pin-fin channels consistently provide the highest $\eta \times$ EAR values as seen in Fig. 8-b due to the large EAR for the present test channels. When the application can provide the sufficient pressure potential to overcome the large increase in f, the scale-roughened pin-fin channel can be selected for further improvements in HTE impact and thermal performance with EAR considered.

4. Conclusions

This experimental study was motivated by the need to further elevate the HTE performances over the endwalls of pin-fin channels. A novel compound HTE measure that consolidates the coherent scale imprints and the pin-fin array was devised with their performances of $\overline{Nu}/Nu_\infty$, f/f_∞, η and $\eta \times$ EAR comparatively examined in the Re range of 1000–30000 for both forward and backward flows. The following concluding remarks are accordingly emerged.

1. While the $\overline{Nu}/Nu_\infty$ ratios for the smooth-walled pin-fin channels fall in the ranges of 2–3.2 in turbulent regime, the present scale-roughened pin-fin channels considerably elevate the $\overline{Nu}/Nu_\infty$ ratios to 5.16–22 in the Re range of 1000–30000. With $Re \leq 2000$, $\overline{Nu}/Nu_\infty$ for the present scale-roughened pin-fin channels with forward and backward flows are respectively elevated to 14.9–22 and 11.6–17.1 with $S/D_P = 1$ and 6.74–11.2 and 5.16–8.7 with $S/D_P = 2$. With $3000 \leq Re \leq 30\,000$, the $\overline{Nu}/Nu_\infty$ ratios detected from the present test channels with forward and backward flows reach 8.6–4.98 and 6.7–3.9 with $S/D_P = 1$ and 4.8–4.1 and 3.7–3.4 with $S/D_P = 2$.
2. The high pressure drops developed in the present test channels are inherited from the pressure drops induced by the pin-fin arrays rather than the scale imprints. The significant elevations in f/f_∞ ratios for the present test channels have suppressed the HTE impacts and led to the lowest η values in the comparative group collected in Fig. 8a.
3. As an HTE measure for pin-fin channels, the scale-roughened endwalls only attribute to the insensible pressure-drop penalty relative to the f factors induced by the pin-fin array but can stimulate significant $\overline{Nu}/Nu_\infty$ elevations with the most effective augmentations in heat transfer power evaluated as $\eta \times$ EAR as compared in Fig. 8b.
4. For design applications, two sets of empirical correlations that evaluate $\overline{Nu}$ and f using Re as the determined variable are derived for two scale-roughened pin-fin channels with $S/D_P = 1$ and 2 under forward and backward flow conditions.

Acknowledgement

This work was funded by the National Science Council, Taiwan, R.O.C. under the grant number, NSC 97-2221-E-022-013-MY3. The helps during the revised process by our research student Yi-An Lan is acknowledged.

References

[1] M.K. Chyu, V. Natarajan, Heat transfer on the base surface of three-dimensional protruding elements. Int. J. Heat Mass Transfer 39 (1996) 2925–2935.
[2] S.Y. Won, G.I. Mahmood, P.M. Ligrani, Spatially-resolved heat transfer and flow structure in a rectangular channel with pin fins. Int. J. Heat Mass Transfer 47 (2004) 1731–1743.
[3] G.J. Van Fossen, Heat-transfer coefficients for staggered arrays of short pin-fins. ASME Eng. Gas Turbines Power 104 (1982) 268–274.
[4] M.K. Chyu, Y.C. Hsing, T.I.-P. Shih, V. Natarajan, Heat transfer contributions of pins and endwall in pin-fin arrays: effects of thermal boundary condition modeling. ASME J. Turbomachinery 121 (1999) 257–263.
[5] D.E. Metzger, R.A. Berry, J.P. Bronson, Developing heat transfer in rectangular ducts with staggered arrays of short pin fins. ASME J. Heat Transfer 104 (1982) 700–706.
[6] M.K. Chyu, Heat transfer and pressure drop for short pin-fin arrays with pin-endwall fillet. ASME J. Heat Transfer 112 (1990) 926–932.
[7] D.E. Metzger, C.D. Fan, S.W. Haley, Effects of pin shape and array orientation on heat transfer and pressure loss in pin arrays. ASME J. Eng. Gas Turbines Power 106 (1984) 252–257.
[8] N. Sahiti, A. Lemouedda, D. Stojkovic, F. Durst, E. Franz, Performance comparison of pin fin in-duct flow arrays with various pin cross-sections. Appl. Thermal Eng. 26 (2006) 1176–1192.
[9] E.M. Sparrow, V.B. Grannis, Pressure drop characteristics of heat exchangers consisting of arrays of diamond-shaped pin fins. Int. J. Heat Mass Transfer 34 (1991) 589–600.
[10] M.K. Chyu, C.H. Yen, S. Siw, Comparison of heat transfer from staggered pin fin arrays with circular, cubic and diamond shaped element, GT2007-28306, ASME Turbo Expo (2007) May 14–17, Montreal, Canada.
[11] N. Sahiti, F. Durst, P. Geremia, Selection and optimization of pin cross-sections for electronics cooling. Appl. Thermal Eng. 27 (2007) 111–119.
[12] B.A. Jubran, M.A. Hamdan, R.M. Abdualh, Enhanced heat transfer, missing pin and optimization for cylindrical pin fin arrays. ASME J. Heat Transfer 115 (1993) 576–583.
[13] M.K. Chyu, V. Natarajan, Effect of flow angle-of-attach on the local heat/mass transfer distributions from a wall-mounted cube. ASME J. Heat Transfer 116 (1994) 552–560.
[14] M.K. Chyu, E.O. Oluyede, Moon, H.-K., Heat transfer on convective surfaces with pin-fins mounted in inclined angles, GT2007-28138, ASME Turbo Expo May 14–17, (2007) (Montreal, Canada).
[15] M.B. Dogruoz, M. Urdaneta, A. Ortega, Experiments and modeling of the hydraulic resistance and heat transfer of in-line square pin fin heat sink with top by-pass flow. Int. J. Heat Mass Transfer 48 (2005) 5058–5071.
[16] S.W. Chang, T.L. Yang, C.C. Huang, K.F. Chiang, Endwall heat transfer and pressure drop in rectangular channels with attached and detached circular pin-fin array. Int. J. Heat Mass Transfer 51 (2008) 5247–5259.
[17] S.W. Chang, T.-M. Liou, M.H. Lu, Heat transfer of rectangular narrow channel with two opposite scale-roughened walls. Int. J. Heat Mass Transfer 48 (2005) 3921–3931.
[18] T.-M. Liou, S.W. Chang, J.S. Chen, C.Y. Chan, Fluid flow inside a rectangular duct with two opposite walls roughened by deepened scales, GT2009–53902, Proceedings of ASME Turbo Expo (2009) June 8–12, 2009, (Orlando, USA).
[19] Editorial Board of ASME, J. Heat Transfer, Journal of heat transfer policy on reporting uncertainties in experimental measurements and results. ASME J. Heat Transfer 115 (1993) 5–6.
[20] S.W. Chang, T.-M. Liou, K.F. Chiang, G.F. Hong, Heat transfer and pressure drop in rectangular channel with compound roughness of V-shaped ribs and deepened scales. Int. J. Heat Mass Transfer 51 (2008) 457–468.
[21] J.C. Han, Y.M. Zhang, C.P. Lee, Augmented heat transfer in square channels with parallel, crossed, and V-shaped angled ribs. ASME J. Turbomachinery 113 (1991) 590–597.
[22] M.E. Taslim, T. Li, D. Kercher, Experimental heat transfer and friction in channels roughened with angle, V-shaped, and discrete ribs on two opposite walls. ASME J. Turbomachinery 118 (1996) 20–28.
[23] X. Gao, B. Sundén, Heat transfer and pressure drop measurements in rib-roughened rectangular ducts. Exp. Thermal Fluid Sci. 24 (2001) 25–34.
[24] A. Zukauskas, R. Ulinskas, Efficiency parameters for heat transfer in tube banks. Heat Transfer Eng. 6 (1985) 19–25.